ELSEVIER

Biophysical Chemistry 134 (2008) 200–206

Biophysical Chemistry

http://www.elsevier.com/locate/biophyschem

Role of spin state on the geometry and nuclear quadrupole resonance parameters in hemin complex

Hadi Behzadi [a], David van der Spoel [b], Mehdi D. Esrafili [a], Gholam Abbas Parsafar [c], Nasser L. Hadipour [a,d,*]

[a] Department of Chemistry, Tarbiat Modares University, P.O. Box: 14115-175, Tehran, Iran
[b] Department of Cell and Molecular Biology, Biomedical Centre, Box, 596, Uppsala University, SE-75 124 Uppsala, Sweden
[c] Department of Chemistry, Sharif University of Technology, Tehran, Iran
[d] Institute of Chemistry, Academia Sinica,128 Yen-Chiu-Yuan Rd. Nankang, Taipei 11529, Taiwan

Received 20 December 2007; received in revised form 13 February 2008; accepted 13 February 2008
Available online 4 March 2008

Abstract

Theoretical calculations of structural parameters, ^{57}Fe, ^{14}N and ^{17}O electric field gradient (EFG) tensors for full size-hemin group have been carried out using density functional theory. These calculations are intended to shed light on the difference between the geometry parameters, nuclear quadrupole coupling constants (QCC), and asymmetry parameters (η_Q) found in three spin states of hemin; doublet, quartet and sextet. The optimization results reveal a significant change for propionic groups and porphyrin plane in different spin states. It is found that all principal components of EFG tensor at the iron site are sensitive to electronic and geometry structures. A relationship between the EFG tensor at the ^{14}N and ^{17}O sites and the spin state of hemin complex is also detected.
© 2008 Elsevier B.V. All rights reserved.

Keyword: Hemin; Density functional theory; Electric field gradient tensor; Nuclear quadrupole coupling constants; Asymmetry parameter

1. Introduction

The heme group plays a vital role in biological systems. It is encountered as an active site which determines the biological activities of some proteins. The heme group present in oxygen transport proteins, hemoglobin and myoglobin, metabolizing enzymes such as peroxidase, and enzymes catalyzing important redox reactions in cytochrome [1,2] is the main active site which controls a wide variety of chemical reactions. Hence, understanding properties of heme group, by probing chemical environment of the heme active site, is of great importance for studying catalytic and structural role of these proteins [3–10].

The electric field gradient (EFG) tensors arisen at the sites of quadrupole nuclei are important physical parameters to gain insight to chemical environment and molecular structure. Those nuclei with spin angular momentum greater than one-half ($I > 1/2$) are quadrupole and have electric quadrupole moment, eQ, which can interact with the EFG tensor [11]. Strength of this interaction depends on the magnitude of eQ and the EFG eigenvalues that can be measured experimentally by nuclear quadrupole resonance (NQR) spectroscopy. As for the high sensitivity to the electrostatic environment of nuclei, electronic structures and intermolecular interactions, such as hydrogen bonding (HB), can produce a significant influence on the EFG tensors. The high level quantum mechanics calculations yield the EFG tensors in principal axis system, PAS, which can be converted to NQR measurable parameters: nuclear quadrupole coupling constant (QCC), and asymmetry parameter (η_Q).

In the present work, a full-size heme group, with one water as the fifth ligand, Ferriprotoporphyrin IX, hemin, was studied (Fig. 1). It is to be noted that we considered specific protonated state, one propionic groups as protonated and one deprotonated. Such hemin complex is derived from hemoglobin degradation in

* Corresponding author. Department of Chemistry, Tarbiat Modares University, P.O. Box: 14115-175, Tehran, Iran. Tel.: +98 2188011001 3495; fax: +98 2188009730.
E-mail address: hadipour@modares.ac.ir (N.L. Hadipour).

0301-4622/$ - see front matter © 2008 Elsevier B.V. All rights reserved.
doi:10.1016/j.bpc.2008.02.011

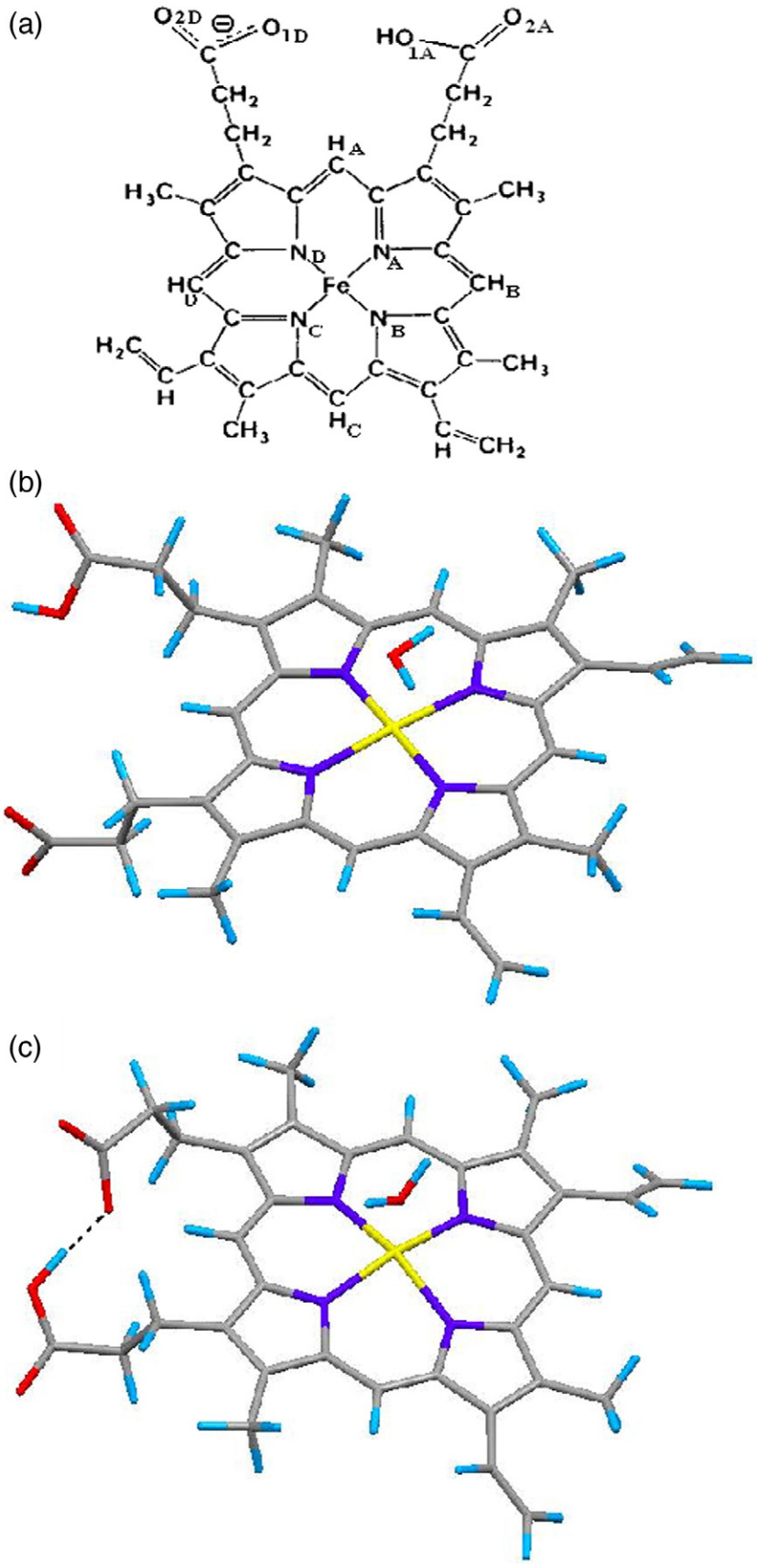

Fig. 1. (a) Chemical structure of the heme group, (b) optimized structure of hemin complex in $M=2$ and (c) optimized structure of hemin complex with one water molecule $M=4$, 6 spin states.

pathogenic blood stage of malaria parasite. The exact p*K*a values of the two propionates are not definitively known, but for hemozoin formation (non-toxic form of heme for parasite), it is necessary for one to be protonated and one unprotonated. The pH dependence hemozoin forming studies by Egan et al. indicate that only mono-protonated hemin species is active [12–14]. Therefore, our model differs from the most previously used in the literature by considering the full-size heme and one protonated state instead of both protonated or deprotonated of propionic groups. Numerous experimental techniques, including X-ray crystallography, mössbauer, EPR, and nuclear magnetic resonance, NMR, spectroscopies have been applied to study the heme group and iron–porphyrin systems in different spin states [15–18]. Furthermore, a number of pioneering quantum mechanical calculations with the density functional theory, DFT, approach has been reported for different spin states of model iron–porphyrin systems [5,19,20]. With this knowledge, geometry of hemin group was optimized in order to investigate the relation between the structure and relative spin state energies in its doublet, quartet, and sextet spin states. Optimizations were performed using density functional theory, DFT, approach. For systematic study purposes, the firstly optimized hemin structures were used for natural bonding orbitals (NBO) analysis and EFG tensors calculations at the ^{57}Fe, ^{17}O, and ^{14}N nuclei. As computed EFG eigenvalues, q_{xx}, q_{yy} and q_{zz}, were converted to those experimentally measurable NQR parameters, nuclear quadrupole coupling constants, QCC and asymmetry parameters, η_Q.

2. Computational details

All calculations were performed using Gaussian 98 suite of programs [21]. The heme structure in Human Carbonmonoxy–Haemoglobin (PDB code: 1IRD) has been applied to initialize the geometry optimization. Hydrogen atoms and water molecule were added using the PYMOL package [22]. Optimizations with no constraints were performed in doublet, quartet, and sextet spin states at DFT level by using the B3LYP method. For geometry optimization, the Lanl2dz and 3–21G* basis sets were used for Fe and other atoms, respectively. This approach has been successfully used to optimization of heme model complexes of cytochrome [2,23]. Then, the EFG and NBO calculations were performed by using DFT/B3LYP method on the geometry optimized structure at different spin states. These calculations were used by using the Lanl2dz basis set for Fe and 6–311+G* for other atoms.

Quantum chemical calculations yield principal components of the EFG tensor, q_{ii}, in atomic unit (1 au = 9.717365×10^{21} V m^{-2}). The calculated q_{ii} values were used to obtain the nuclear quadrupole coupling tensors, QCC, and asymmetry parameters, η_Q, from the equations:

$$\mathrm{QCC(MHz)} = e^2 Q q_{zz}/h \tag{1}$$

$$\eta_Q = \left|\frac{q_{yy}-q_{xx}}{q_{zz}}\right|, \qquad 0\le\eta_Q\le1 \tag{2}$$

where the standard values of eQ reprted by Pyykkö were employed [24]:eQ(^{57}Fe) = 160.0 mb, eQ(^{17}O) = −25.58 mb, and eQ(^{14}N) = 20.44 mb.

3. Results and discussion

3.1. Geometry optimizations

The DFT/B3LYP optimized structures of hemin complexes in doublet, quartet, and sextet spin states are shown in Fig. 1. Besides, the main features of optimized geometry parameters and relative energies are presented in Table 1. State with M=4 multiplicity was found to have the minimum energy level among others. The ground state quartet found here is in accordance with a series studies of five coordinated intermediated spin state Fe(III) porphyrinates [25–28] and theoretical prediction reported by Romanova and Krasnov for iron–porphyrin model of heme [3]. The most significant differences between the three spin states lie in the iron–axial ligand distance and conformation of propionic groups. The four iron–nitrogen distances are nearly equal, $r_{ave(Fe-N)}$=2.012, 1.991, 2.037 Å for doublet, quartet, and sextet spin state, respectively. The obtained values are comparable to experimental data (2.00±0.05 Å) observed in high resolution X-ray heme structures in 1CXT and 1YTC [8]. The Fe–water distance is significantly modified in different spin states. In sextet spin state, the Fe atom is situated out of the porphyrin plane and Fe–OW distance has the smallest value $R_{(Fe-OW)}$=2.025 Å (compared to 2.275 Å and 2.112 Å in M=2 and M=4, respectively). The CH_A–Fe–CH_C and CH_B–Fe–CH_D bond angles were used to measure the Fe atom displacement from the porphyrin plane. The $R_{(Fe-OW)}$=2.112 Å value, optimized for intermediate spin state, is closest to 2.09 Å value, reported experimentally for ferric–porphyrin diaquo complexes [29].

Conformational changes in propionic groups is another unique feature of geometry optimization in the three spin multiplicities. In doublet spin state two propionic groups lie far from each other while in quartet and sextet spin states, the two groups are much closer and can generate O–H···O hydrogen bond (HB) interaction, transferring a proton from O1A to O1D. The HB distances, $R_{(O1A-O1D)}$, are 2.515 Å and 2.518 Å in quartet and sextet spin states, respectively. Kumar et al. also reported a similar HB formation, C–H···O HB type, in the heme moiety of cytochrome *C* [2]. It must be mentioned that the energy of a moderate O–H···O interaction is 4–15 kcal/mol [30]. Therefore, the obtained energy difference among the spin states is too large to be accounted for simply by H-bonding interactions. All the facts mentioned above suggest that electronic structure and structural parameters are significantly dependent to spin state of hemin complex.

3.2. Electric field gradient tensors

Tables 2–4 indicate the calculated ^{57}Fe, ^{14}N, and ^{17}O nuclear quadrupole coupling tensors and Fe (3d) population for the three spin states of hemin. In the following sections, ^{57}Fe, ^{14}N, and ^{17}O EFG results will be discussed separately.

3.2.1. ^{57}Fe electric gradient tensors

The calculated ^{57}Fe electric field gradient tensor, QCC, and η_Q values for M=2, 4, and 6 spin states of hemin are shown in Table 2. As it is clear at the first glance, ^{57}Fe electric field gradient tensor is significantly dependent on the spine states. It must also

Table 1
Some selected bond distances (Å), bond angles (°), and total energies (eV) values for optimized structures of hemin in different spin states

Parameters	$M=2$	$M=4$	$M=6$
$R_{(Fe–OW)}$	2.275	2.112	2.025
$R_{(Fe–NA)}$	2.005	1.995	2.029
$R_{(Fe–NB)}$	2.019	1.994	2.045
$R_{(Fe–NC)}$	2.019	1.995	2.048
$R_{(Fe–ND)}$	2.006	1.980	2.026
$R_{(Fe–N_{Average})}$	2.012	1.991	2.037
$R_{(CGA–O1A)}$	1.391	1.330	1.330
$R_{(CGA–O2A)}$	1.223	1.238	1.239
$R_{(CGD–O1D)}$	1.277	1.338	1.339
$R_{(CGD–O2D)}$	1.291	1.234	1.234
$R_{(O1A–O1D)}$	4.777	2.515	2.518
$R_{(O1A–H1A)}$	0.998	1.438	1.441
∠Fe–OW–HW1	95.065	111.723	119.143
∠Fe–OW–HW1	94.718	109.402	127.069
∠CHA–Fe–CHC	176.113	176.233	168.067
∠CHB–Fe–CHD	177.675	172.749	165.411
∠FE–OW–HW1	94.718	111.723	127.070
∠FE–OW–HW2	95.096	109.402	119.143
ΔE, eV	3.41	0.00	27.40

be noted that EFG calculations at the iron site of hemin reflect the spatial distribution of electrons around the core which can be divided mainly into two parts [4,31]. The largest may be attributed to valence electrons, q_{val} which results from unequal electron population, particularly in Fe (3d) orbitals. This contribution is proportional to the Fe (3d) orbital anisotropy defined as followed:

$$\Delta n_d = n\left(d_{x^2-y^2}\right) + n\left(d_{xy}\right) - n\left(d_{z^2}\right) - \frac{1}{2}n\left(d_{xz}\right) - \frac{1}{2}n\left(d_{yz}\right).$$

The second term contributes to the external lattice, q_{lat}, which is present when the iron nucleus is located in non-spherical environment produced by the iron–ligand overlap. As

Table 2
Calculated ^{57}Fe, and ^{14}N electric field gradient tensors for different spin states of hemin [a]

Nuclei	Spin state	q_{xx}	q_{yy}	q_{zz}	QCC	η_Q
^{57}Fe	$M=2$	−0.367	−0.718	1.085	40.08	0.32
	$M=4$	0.976	1.192	−2.168	−81.56	0.10
	$M=6$	0.491	0.588	−1.080	−40.63	0.09
NA	$M=2$	0.160	0.318	−0.478	−1.95	0.33
	$M=4$	0.108	0.311	−0.420	−1.72	0.48
	$M=6$	0.180	0.285	−0.464	−1.90	0.23
NB	$M=2$	0.126	0.345	−0.472	−1.93	0.46
	$M=4$	0.132	0.316	−0.448	−1.83	0.41
	$M=6$	0.169	0.317	−0.486	−1.99	0.30
NC	$M=2$	0.160	0.323	−0.484	−1.98	0.34
	$M=4$	0.127	0.318	−0.445	−1.82	0.43
	$M=6$	0.190	0.299	−0.490	−2.00	0.22
ND	$M=2$	0.135	0.336	−0.471	−1.92	0.43
	$M=4$	0.102	0.322	−0.424	−1.73	0.52
	$M=6$	0.161	0.298	−0.460	−1.88	0.30
Exp. [b]		0.219	0.309	−0.528	−2.54	0.17

[a] Calculated q_{ii} components and QCC values in atomic unit and MHz, respectively.
[b] Experimental values for nitrogen in three-coordinated imidazole [37].

Table 3
Fe (3d) population for the spin states of hemin

Population	$M=2$	$M=4$	$M=6$
$n(d_{xy})$	0.669	0.972	1.323
$n(d_{xz})$	1.726	1.140	1.192
$n(d_{yz})$	1.131	1.147	1.175
$n(d_{x^2-y^2})$	1.930	1.900	1.035
$n(d_{z^2})$	1.191	1.171	1.209
n_d	6.647	6.33	5.93
Δn_d	−0.02	0.18	−0.04

concluded from Table 3 data, there is negligible amount of anisotropy resulting from Fe (3d) orbitals in doublet and sextet spin states, $\Delta n_d=-0.02$ for $M=2$ and $\Delta n_d=-0.04$ for $M=6$, and hence, valence electrons have no significant effect on the EFG. Thus, overlap with the porphyrin nitrogen and water influences the field gradient at Fe site, resulting in lattice effects. In contrast to $M=2$ and $M=6$ spin states, there is a noticeable

Table 4
Calculated relative orientation of EFG tensors at ^{14}N sites in different spin states of hemin

Nuclei	q_{ii}	Spin state	Angle of the principal axes system/°		
			x	y	z
NA	q_{xx}	$M=2$	86.62	81.58	9.11
		$M=4$	50.17	39.97	87.26
		$M=6$	83.63	84.93	8.15
	q_{yy}	$M=2$	45.38	45.84	81.61
		$M=4$	88.35	85.05	5.20
		$M=6$	13.90	78.33	82.71
	q_{zz}	$M=2$	44.82	45.40	86.48
		$M=4$	39.88	50.47	85.57
		$M=6$	77.70	12.84	86.38
NB	q_{xx}	$M=2$	86.45	81.86	8.89
		$M=4$	37.22	53.46	83.87
		$M=6$	81.66	89.58	8.35
	q_{yy}	$M=2$	45.16	46.02	81.47
		$M=4$	88.19	82.22	7.99
		$M=6$	38.47	52.37	83.15
	q_{zz}	$M=2$	35.06	45.13	86.75
		$M=4$	52.84	37.63	84.89
		$M=6$	25.18	37.74	85.25
NC	q_{xx}	$M=2$	87.16	84.66	6.07
		$M=4$	52.60	37.46	88.30
		$M=6$	88.02	89.53	1.98
	q_{yy}	$M=2$	45.96	44.09	88.13
		$M=4$	89.99	87.85	2.14
		$M=6$	52.79	37.23	89.18
	q_{zz}	$M=2$	44.18	46.40	84.24
		$M=4$	37.40	52.63	88.69
		$M=6$	37.28	52.77	88.14
ND	q_{xx}	$M=2$	82.50	89.45	7.52
		$M=4$	35.91	54.18	87.74
		$M=6$	85.78	85.47	6.17
	q_{yy}	$M=2$	45.95	44.61	84.35
		$M=4$	88.73	87.90	2.43
		$M=6$	36.48	54.18	83.92
	q_{zz}	$M=2$	45.03	45.39	85.05
		$M=4$	54.11	35.90	89.04
		$M=6$	53.84	36.19	88.83

valence contribution to the EFG in $M=4$ with $\Delta n_d=0.18$. Besides, the lattice contribution from the Fe–ligand overlap is more in $M=4$ due to the shorter Fe–N distances in quartet spin state. Consequently, the two mentioned above contributions have found to effect the nuclear quadrupole coupling by $|\Delta QCC| \cong 40$ MHz for $M=4$ spin state. Furthermore, the calculated EFG components, q_{ii}, and asymmetry parameters reproduce experimental values reported for heme proteins and model systems [19,32–34].

Finally, it is worth noting that in addition to the principal eigenvalues of the EFG tensor, the theoretical calculations also give the orientation of the EFG eigenvectors in the molecular axes. From calculation based on the B3LYP/6–311+G*, it was found that for $M=2$ spin state, q_{zz} component approximately lies in the porphyrin plane, whereas the q_{xx} and q_{yy} components make 51.70° and 38.35° along Fe–OW bond direction, respectively (Fig. 2). For the $M=4$ and 6 spin states, the orientation of EFG principal components is slightly different. As depicted in Fig. 2, q_{zz} has a tendency to orientate along the Fe–OW bond while both q_{xx} and q_{yy} align the porphyrin plane.

3.2.2. ^{14}N electric gradient tensors

The calculated ^{14}N EFG tensors for four nitrogen atoms in hemin structure; NA, NB, NC and ND are presented in Table 2. It can be inferred that spin state of hemin protein follows a regular pattern for the QCC(^{14}N) and parameters. As mentioned above, spin state has no significant influence on the Fe–N bond distances. However, such little changes in inter-atomic Fe–N interactions have potential to affect charge distribution around the nitrogen sites so, the order of QCC(^{14}N) is obtained to be $M=5/2>1/2>3/2$, which is consistent with the bond distance. Such kind of structural sensitivity is found for hydrogen bonded systems, in which QCC(^{14}N) decreases as N···O bond shortens [35,36]. Moreover, based on EFG tensor calculations, asymmetry parameter for the four nitrogen sites are in the 0.22–0.52 range. However, the calculated ^{14}N EFG tensors are consistent with experimental values reported for three-coordinated imidazole [37]. Table 4 shows the relative orientations of ^{14}N EFG principal components in hemin complexes. In each spin state, almost similar orientation is detected for the four porphyrin nitrogens. However, for $M=2$ and 6, q_{xx} component approximately

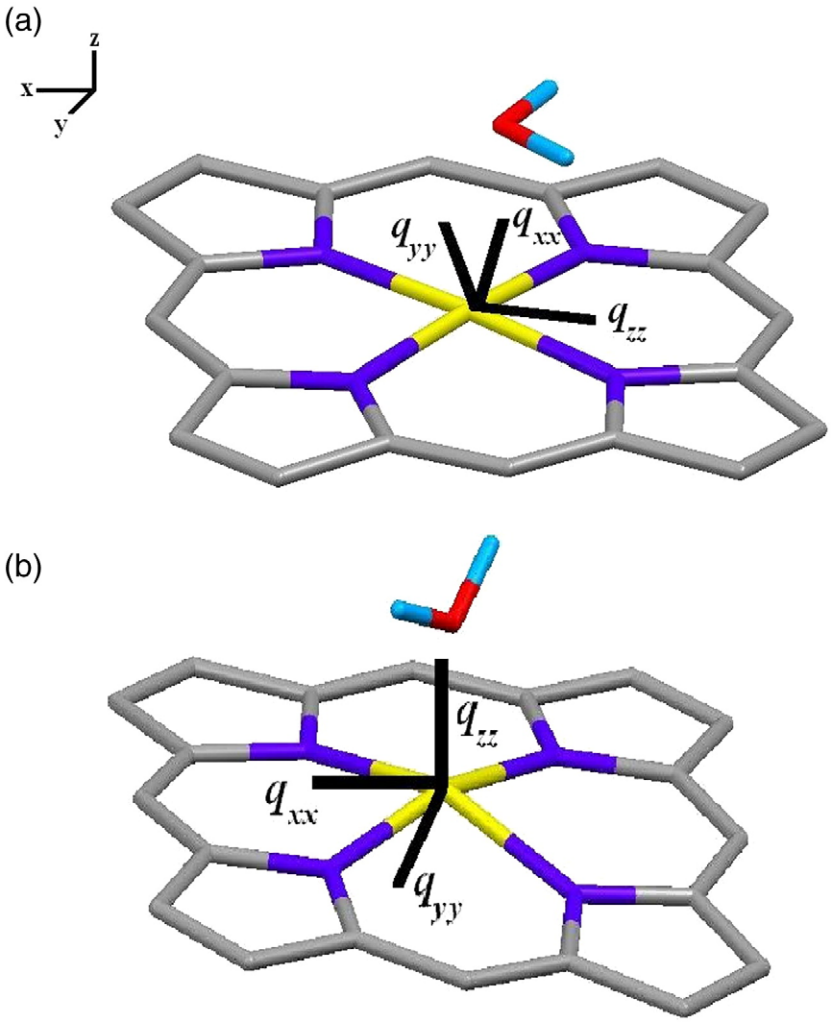

Fig. 2. EFG tensor orientations for ^{57}Fe nucleus of hemin molecule in different spin states. (a) $M=2$ and (b) $M=4$ and $M=6$.

Table 5
Calculated ^{17}O EFG tensors for different spin states of hemin

Nuclei	Spin state	q_{xx}	q_{yy}	q_{zz}	C_Q	η_Q
^{17}O1A	M=2	0.336	1.279	−1.615	−9.71	0.58
	M=4	0.153	1.087	−1.240	−7.46	0.75
	M=6	0.154	1.086	−1.241	−7.46	0.75
^{17}O2A	M=2	−0.722	−0.893	1.615	9.71	0.11
	M=4	−0.756	−0.842	1.598	9.61	0.05
	M=6	−0.755	−0.841	1.596	9.60	0.05
^{17}O1D	M=2	0.407	0.491	−0.898	−5.40	0.09
	M=4	0.528	0.861	−1.389	−8.35	0.24
	M=6	0.533	0.857	−1.390	−8.36	0.23
^{17}O2D	M=2	0.091	0.858	−0.949	−5.71	0.81
	M=4	−0.813	−0.853	1.665	10.01	0.02
	M=6	−0.812	−0.847	1.658	9.97	0.02
^{17}OW	M=2	−0.124	−1.575	1.700	10.22	0.85
	M=4	−0.185	−1.553	1.738	10.45	0.79
	M=6	−0.330	−1.600	1.930	11.61	0.66

Calculated q_{ii} components and QCC values in atomic unit and MHz, respectively.

lies in the Fe–OW bond direction and q_{yy} and q_{zz} are directed in porphyrin plane, while in the M=4 the q_{xx} and q_{zz} components are approximately in the porphyrin plane and q_{yy} tends to lie in Fe–OW direction.

3.2.3. ^{17}O electric gradient tensors

In this section, we focus on the quantum chemical ^{17}O EFG tensor calculations for propionic and water oxygen in full-size aqua hemin complex at different spin states. Wu et al. have recently showed DFT calculations to be reliable for ^{17}O EFG in organic molecules [38–41]. In contrast to ^{14}N, structural effects on ^{17}O EFG tensors may be more complicated (Table 5). As stated earlier in geometry optimization section, conformation of propionic groups is different in various spin states resulting different values of ^{17}O EFG tensors. It was also mentioned that one of the propionic groups is not neutral. According to Table 5, in doublet spin state the QCC(^{17}O1D) is close to the QCC (^{17}O2D) and far from the QCC(^{17}O1A) and QCC(^{17}O2A) values. For example, the calculated QCC(^{17}O1D) is smaller than the QCC(^{17}O1A) by 4.31 MHz. Both O1A and O2A belong to protonated propionic group of hemin while O1D and O2D contribute to non-protonated one. While moving from M=2 to M=4 spin state, HB formation makes ΔQCC(^{17}O)= 2.25 and 2.95 MHz for O1A and O1D, respectively. As for similar structures of propionic groups in quartet and sextet spin states, computed QCC(^{17}O) and values are consistent. There are no experimental data available for ^{17}O NQR parameters in hemin propionic groups and our results need to be confirmed by future experiments. However, comparison of the reported ^{17}O NQR parameters for O1A and O1D with those of experimental NQR parameters for DL-glutamic acid (QCC=7.24, 7.33 MHz and=0.72, 0.23) can enhance the validity of our work [42].

The EFG tensors of water oxygen also show sensitivity to spin state. As the Fe–OW distance reduces from lower to higher spin states, the QCC(^{17}OW) value increases and the parameter decreases.

4. Conclusions

The geometry and EFG tensors of hemin complex were studied via density functional theory. According to the results obtained in this investigation, spin state of hemin complex has a remarkable influence on the geometry parameters and EFG tensors at ^{57}Fe, ^{14}N and ^{17}O sites. The comparison of different spin states revealed that for the M=4 and 6 spin states, two propionic groups form a O–H···O intra-molecular hydrogen bonding interaction. It is also concluded that EFG tensors of ^{57}Fe, ^{14}N and ^{17}O nuclei are appropriate parameters to characterize the electronic structures and properties of hemin complex in various spin states. The theoretically calculated ^{57}Fe nuclear quadrupole coupling constant for the M=2, 4 and 6 spin states, are predicted to be experimentally distinguishable: $|\Delta QCC| \cong 40$ MHz. EFG tensors at the nitrogen nuclei exhibit a proper pattern due to the regularity of Fe–N bond distances. It was also shown that hydrogen bonding interaction has a significant influence on QCC (^{17}O) and η_Q(^{17}O) values.

References

[1] A.C. Cotton, G. Wilkinson, Advanced Inorganic Chemistry, 6th ed.John Wiley & Sons, New York, 1999.
[2] A. Kumar, P.C. Mishra, C.S. Verma, V. Renugopalakrishnan, Density functional study of the hemin moiety of cytochrome *C*, Int. J. Quant. Chem. 102 (2005) 1002–1009.
[3] T.A. Romanova, P.O. Krasnov, Ab initio and post-ab initio quantum chemical study of the hemin spin states in electron transfer reactions, Chem. Phys. Lett., 420 (2006) 281–285.
[4] D. Rutkowska-Zbik, M. Witko, G. Stochel, Theoretical density functional theory studies on interactions of small biologically active molecules with isolated hemin group, J. Comput. Chem. 28 (2007) 825–831.
[5] D.M.A. Smith, Michel Dupuis, Erich R. Vorpagel, T.P. Straatsma, Characterization of electronic structure and properties of a bis(histidine) hemin model complex, J. Am. Chem. Soc. 125 (2003) 2711–2717.
[6] J. Maréchal, G. Barea, F. Maseras, A. Lledós, L. Mouawad, D. Pérahia, Theoretical modeling of the hemin group with a hybrid QM/MM method, J. Comput. Chem. 21 (2000) 282–294.
[7] V. Guallar, B. Olsen, The role of the hemin propionates in hemin biochemistry, J. Inorg. Biochem., 100 (2006) 755–760.
[8] F. Autenrieth, E. Tajkkhorshid, J. Baudry, Z. Luthey-Schulten, Classical force field parameters for the hemin prostheticgroup of cytochrome *C*, J. Comput. Chem. 25 (2004) 1613–1622.
[9] R. Wang, S.P. de Visser, How does the push/pull effect of the axial ligand influence the catalytic properties of Compound I of catalase and cytochrome P450? J. Inorg. Biochem. 101 (2007) 1464–1472.
[10] A.E. Medlock, T.A. Dailey, T.A. Ross, H.A. Dailey, W.N. Lanzilotta, A π-helix switch selective for porphyrin deprotonation and product release in human ferrochelatase, J. Mol. Biol., 373 (2007) 1006–1016.
[11] C.P. Slichter, Principles of Magnetic Resonance, Harper & Row, London, 1992.
[12] T.J. Egan, J.Y.-J. Chen, K.A. de Villiers, T.E. Mabotha, K.J. Naidoo, K.K. Ncokazi, S.J. Langford, D. McNaughton, S. Pandiancherri, B.R. Wood, Haemozoin (β-haematin) biomineralization occurs by self-assembly near the lipid/water interface, FEBS Lett. 580 (2006) 5105–5110.
[13] T.J. Egan, M.G. Tshivhase, Kinetics of *b*-haematin formation from suspensions of haematin in aqueous benzoic acid, Dalton Trans. (2006) 5024.
[14] T.J. Egan, W.W. Mavuso, K.K. Ncokazi, The mechanism of β-hematin formation in acetate solution. Parallels between hemozoin formation and biomineralization processes, Biochemistry 40 (2001) 204.
[15] A.Y. Alontaga, R.A. Bunce, A. Wilks, M. Rivera, ^{13}C NMR spectroscopy of core heme carbons as a simple tool to elucidate the coordination state of ferric high-spin heme proteins, Inorg. Chem. 45 (2006) 8876.

[16] A.Y. Alontaga, R.A. Bunce, A. Wilks, M. Rivera, ^{13}C and ^{15}N NMR studies of iron-bound cyanides of heme proteins and related model complexes: sensitive probe for detecting hydrogen-bonding interactions at the proximal and distal sides, Inorg. Chem. 45 (2006) 6816–6827.
[17] S.H. Kim, C. Aznar, M. Brynda, L.A. "Pete" Silks, R. Michalczyk, C.J. Unkefer, W.H. Woodruff, R.D. Britt, An EPR, ESEEM, structural NMR, and DFT study of a synthetic model for the covalently ring-linked tyrosine–histidine structure in the heme–copper oxidases, J. Am. Chem. Soc. 126 (2004) 2328–2338.
[18] M. Sharrock, E. Munck, P.G. Debrunner, V. Marshall, J.D. Lipscomb, I.C. Gunsalus, Mossbauer studies of cytochrome P-450, Biochemistry 12 (1973) 258–265.
[19] Y. Zhang, J.H. Mao, N. Godbout, E. Oldfield, Mossbauer quadrupole splittings and electronic structure in hemin proteins and model systems: a density functional theory investigation, J. Am. Chem. Soc. 124 (2002) 13921–13930.
[20] Y. Zhang, W. Gossman, E. Oldfield, A density functional theory investigation of Fe–N–O bonding in hemin proteins and model systems, J. Am. Chem. Soc. 125 (2003) 16387–16396.
[21] M.J. Frisch, G.W. Trucks, H.B. Schlegel, G.E. Scuseria, M.A. Robb, J.R. Cheeseman, V.G. Zakrzewski, J.A. Montgomery Jr., R.E. Stratmann, J.C. Burant, S. Dapprich, J.M. Millam, A.D. Daniels, K.N. Kudin, M.C. Strain, O. Farkas, J. Tomasi, V. Barone, M. Cossi, R. Cammi, B. Mennucci, C. Pomelli, C. Adamo, S. Clifford, J. Ochterski, G.A. Petersson, P.Y. Ayala, Q. Cui, K. Morokuma, D.K. Malick, A.D. Rabuck, K. Raghavachari, J.B. Foresman, J. Cioslowski, J.V. Ortiz, A.G. Baboul, B.B. Stefanov, G. Liu, A. Liashenko, P. Piskorz, I. Komaromi, R. Gomperts, R.L. Martin, D.J. Fox, T. Keith, M.A. Al-Laham, C.Y. Peng, A. Nanayakkara, C. Gonzalez, M. Challacombe, P.M.W. Gill, B. Johnson, W. Chen, M.W. Wong, J.L. res, C. Gonzalez, M. Head-Gordon, E.S. Replogle, J.A. Pople, Gaussian 98, Gaussian Inc, Pittsburgh PA, 1998.
[22] http://pymol.sourceforge.net/.
[23] M.C. Rosales-Hernández, J. Correa-Basurto, C. Flores-Sandoval, J. Marín-Cruz, E. Torres, J. Trujillo-Ferrara, Theoretical study of hemin derivatives under DFT calculations, J. Mol. Stru.: THEOCHEM, 804 (2007) 81–88.
[24] P. Pyykkö, Spectroscopic nuclear quadrupole moment, Mol. Phys. 99 (2001) 1617–1629.
[25] D.H. Dolphin, J.R. Sams, T.B. Tsin, Intermediate-spin (S=3/2) porphyrinatoiron(III) complexes, Inorg. Chem. 16 (1977) 711.
[26] C.A. Reed, T. Mashiko, S.P. Bentley, M.E. Kastner, W.R. Scheidt, K. Spartalian, G. Lang, The missing heme spin state and a model for cytochrome c¢. The mixed S=3/2, 5/2 intermediate spin ferric porphyrin: perchlorato (*meso*-tetraphenylporphinato) iron(III), J. Am. Chem. Soc. 101 (1979) 2948.
[27] G.P. Gupta, G. Lang, Y.J. Lee, W.R. Scheidt, K. Shelly, C.A. Reed, Spin coupling in admixed intermediate-spin iron(III) porphyrin dimers: crystal structure, Moessbauer, and susceptibility study of Fe(TPP)(B11CH12). C7H8, Inorg. Chem. 26 (1987) 3022.
[28] W.R. Scheidt, D.K. Geiger, C.A. Reed, Susceptibility and Mössbauer study of coupled admixed-spin state in $[Fe(OEP)\ (3\text{-}ClPy)]^+$ dimmers, J. Chem. Phys. 85 (1986) 5212.
[29] W.R. Scheidt, I.A. Cohen, M.E. Kastner, A structural model for hemin in high-spin ferric hemoproteins. Iron atom centering, porphinato core expansion, and molecular stereochemistry of high-spin diaquo(*meso*-tetraphenylporphinato) iron(III) perchlorate, Biochemistry 18 (1979) 3546–3552.
[30] G.A. Jeffrey, An introduction to hydrogen bonding, Oxford University Press, Oxford, U. K., 1997.
[31] M. Grodzicki, H. Flint, H. Winkler, F.A. Walker, A.X. Trautwein, Electronic structure, porphyrin core distortion, and fluxional behavior of bis-ligated low-spin iron(II) porphyrinates, J. Phys. Chem. A 101 (1997) 4202–4207.
[32] F.A. Walker, H. Nasri, I. Turowska-Tyrk, K. Mohanrao, C.T. Watson, N.V. Shokhirev, P.G. Debrunner, W.R. Scheidt, π-acid ligands in iron(III) porphyrinates. Characterization of low-spin bis(*tert*-butylisocyanide)(porphyrinato)iron(III) complexes having $(d_{xz},d_{yz})4(d_{xy})1$ ground states, J. Am. Chem. Soc. 118 (1996) 12109–12118.
[33] W.R. Scheidt, D.K. Geiger, Y.J. Lee, C.A. Reed, G. Lang, On the preparation of five-coordinate (3-chloropyridine)(porphinato)iron(III) complexes, Inorg. Chem. 26 (1987) 1039–1045.
[34] W.R. Scheidt, D.K. Geiger, Y. J Lee, P. Gans, J.C. Marchon, Two salts of bis(ethanol)(*meso*-tetraphenylporphinato)iron(III). Molecular structures and magnetic susceptibilities, Inorg. Chem. 31 (1992) 2660–2663.
[35] R. Ludwig, F. Weinhold, T.C. Farrar, Theoretical study of hydrogen bonding in liquid and gaseous *N*-methylformamide, J. Chem. Phys. 107 (1997) 499–507.
[36] B.F. King, T.C. Farrar, F. Weinhold, Quadrupole coupling-constants in linear $(HCN)_n$ clusters — theoretical and experimental evidence for cooperativity effects in C–H···N hydrogen-bonding, J. Chem. Phys. 103 (1995) 348–352.
[37] G.L. Blackman, R.D. Brown, F.R. Burden, I.R. Elsum, Nuclear quadrupole coupling in the microwave spectrum of imidazole, J. Mol. Spectrosc. 60 (1976) 63–70.
[38] K. Yamada, S. Dong, G. Wu, Solid-state ^{17}O NMR investigation of the carbonyl oxygen electric-field-gradient tensor and chemical shielding tensor in amides, J. Am. Chem. Soc. 122 (2000) 11602–11609.
[39] G. Wu, S. Dong, R. Ida, N. Reen, A solid-state ^{17}O nuclear magnetic resonance study of nucleic acid bases 124 (2002) 1768–1777.
[40] G. Wu, K. Yamada, S. Dong, H. Grondey, Intermolecular hydrogen-bonding effects on the amide oxygen electric-field-gradient and chemical shielding tensors of benzamide, J. Am. Chem. Soc. 122 (2000) 4215–4216.
[41] R. Ida, M. De Clerk, G. Wu, Influence of N–H···O and C–H···O hydrogen bonds on the ^{17}O NMR tensors in crystalline uracil: computational study, J. Phys. Chem. A 110 (2006) 1065–1071.
[42] J.R. Yates, C.J. Pickard, M.C. Payne, Theoretical investigation of oxygen-17 NMR shielding and electric field gradients in glutamic acid polymorphs, J. Phys. Chem. A, 108 (2004) 6032–6037.